# Efficient Algorithms for Tracking Moving Interfaces in Industrial Applications: Inkjet Plotters, Electrojetting, Industrial Foams, and Rotary Bell Painting


**Maria Garzon, Robert I. Saye, and James A. Sethian**

**Abstract** Moving interfaces are key components of many dynamic industrial processes, in which complex interface physics determine much of the underlying action and performance. Level set methods, and their descendents, have been valuable in providing robust mathematical formulations and numerical algorithms for tracking the dynamics of these evolving interfaces. In manufacturing applications, these methods have shed light on a variety of industrial processes, including the design of industrial inkjet plotters, the mechanics of electrojetting, shape and evolution in industrial foams, and rotary bell devices in automotive painting. In this review, we discuss some of those applications, illustrating shared algorithmic challenges, and show how to tailor these methods to meet those challenges.

Moving interfaces are key components of many dynamic industrial processes, whose dynamics are critical to the underlying physics. Examples include turbines, flames and combustion, plastic injection molding, microfluids, and pumping. In each of these examples, complex physics at the interface, such as between a fluid and a moving wall, or through a membrane or a transition region, determines much of the underlying action and performance (Fig. 1).

One approach to propagating interfaces is given by "level set methods". These algorithms to track interfaces in multiple dimensions, couple the driving physics with the interface in a natural way, and smoothly handle topological change due to merger and breaking. They accurately and robustly compute high order solutions

M. Garzon
Department of Applied Mathematics, University of Oviedo, Oviedo, Spain
e-mail: maria@uniovi.es

R. I. Saye
Mathematics Group, Lawrence Berkeley National Laboratory, Berkeley, CA 94720, USA
e-mail: rsaye@lbl.gov

J. A. Sethian (✉)
Department of Mathematics, University of California, Berkeley, California 94720, USA
e-mail: sethian@math.berkeley.edu



T. Chacón Rebollo et al. (eds.), *Recent Advances in Industrial and Applied Mathematics*, ICIAM 2019 SEMA SIMAI Springer Series 1,
https://doi.org/10.1007/978-3-030-86236-7_10

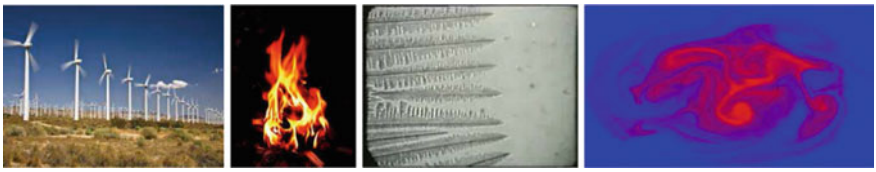


**Fig. 1** Examples of industrial interfaces

to moving interface problems, and are easily discretized using standard techniques, such as finite difference, finite element, and discontinuous Galerkin methods.

The paper is a review of the application of these methods to some industrial problems, and draws from multiple sources [10–17, 26–29, 42–44] to discuss the design of industrial inkjet plotters, jetting and electrojetting devices, industrial foams, and rotary bell spray devices. Rather than extensively focus on the equations or the algorithms, we provide an overview of the approaches, with an emphasis on the results. References are provided for more in-depth discussions.

## 1 Modeling Interface Evolution Using Level Set Methods

Level set methods, introduced in [19], have been used in a large number of applications to track moving interfaces. They are based on both a general mathematical theory as well as a robust numerical methodology, which relies on exchanging the typical Lagrangian perspective on front propagation, in which the front is explicitly tracked, for an Eulerian view in which the moving interface is embedded as a particular level set of a higher dimensional function posed in a fixed coordinate system. The motion of the interface corresponds to solving the evolution of this higher-dimensional function according to a Hamilton-Jacobi-type initial value partial differential equation.

A brief summary is as follows. Consider a moving interface $\Gamma(t)$, parameterized by $N-1$ dimensions. We restrict ourselves to interfaces which are closed and simple, and separate the domain into an "inside" and an "outside". We recast the problem by implicitly defining the moving interface $\Gamma(t)$ propagating in $N-1$ dimensions as the zero level set of the solution to an evolving level set function $\phi(x,t)$, $\phi : \mathbb{R}^N \times t \to \mathbb{R}$, which satisfies a time-dependent partial differential equation. There are many ways to initialize this implicit function: one approach is to let $\phi(x, t=0)$ be the signed distance from the interface $\Gamma(t=0)$, linking the interface to the zero level set.

We assume that the underlying physics specifies a speed $F$ normal to the interface at every point on the interface. Constructing this speed function typically involves solving complex physics both on and off the interface.

Thus, there are two embeddings. First, the interface itself is embedded and implicitly defined through a higher-dimensional function $\phi$. Second, to move the other level sets, we embed the speed $F$ in a higher-dimensional function, known in the literature as the "extension velocity" $F_{ext}$, which defaults to the given speed on the zero level set corresponding to the interface.

## 1.1 Equations of Motion

Here, we review the basic ideas behind the derivation and implementations of level set methods. We follow the derivation and discussion in [35, 36].

We wish to produce an Eulerian formulation for the motion of a hypersurface $\Gamma$ representing the interface and propagating along its normal direction with speed $F$, where $F$ can be a function of various arguments. Let $\pm d(x)$ be the signed distance from the point $x \in \mathbb{R}^N$ to the interface at time $t = 0$. Define a function $\phi(x, t = 0)$ by the equation

$$\phi(x, t = 0) = \pm d(x). \tag{1}$$

By requiring that the zero level set of the evolving $\phi$ (see Fig. 2, left) always match the propagating hypersurface, means that

$$\phi(x(t), t) = 0. \tag{2}$$

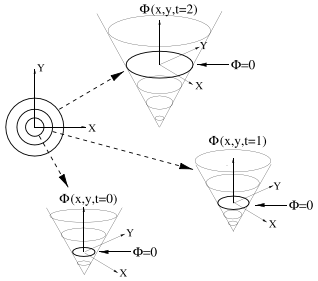


Transformation of front motion into initial value problem. An implicitly defined surface $\phi$, whose ensuing motion satisfies Equation 3, and whose zero level set always matches the motion of the interface.

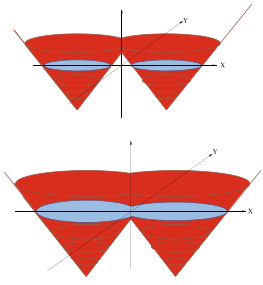

The level surface $\phi$ in red. Top: $\phi = 0$ corresponds to two separate initial fronts. Bottom: Later in time: the interface topology has changed, yielding a single curve as the zero level set.

**Fig. 2** Left: Implicit embedding of level set function. Right: Topological change

By the chain rule, $\phi_t + \nabla\phi(x(t), t) \cdot x'(t) = 0$, Since $x'(t) \cdot \mathbf{n} = F_{ext}$, where $\mathbf{n} = \nabla\phi/|\nabla\phi|$ with extension velocity $F_{ext}$, this yields an evolution equation for $\phi$, namely,

$$\phi_t + F_{ext}|\nabla\phi| = 0, \quad \text{given} \quad \phi(x, t = 0). \tag{3}$$

This is the level set equation introduced by Osher and Sethian [19]. Propagating fronts can develop shocks and rarefactions in the gradient, corresponding to corners and fans in the evolving interface, and numerical techniques designed for hyperbolic conservation laws can be exploited to construct schemes which produce the correct, physically reasonable entropy solution, see [32–34].

There are several advantages to this approach. First, the formulation works in any number of dimensions. Second, topological changes are handled without special attention: fronts split and merge. Third, geometric quantities along the interface can be calculated by taking advantage of the embedding and computing quantities in the fixed Eulerian setting. Fourth, this formulation naturally lends itself to numerical approximations, for example, through finite difference or finite element formulations on the fixed background mesh.

### *1.2 Computational Advances*

Since its introduction, a large number of computational advances have been developed to make this approach efficient, accurate, and economical. These include

- The introduction of adaptive, "narrow band level set methods" [1] which confine computation to a thin band around the zero level set.
- Fast methods to construct extension velocities [2, 25].
- Incorporation of complex physics [3–5], transport of material quantities [6], and methods to handle multi-phase flows with a large number of distinct propagating regions coming together in complex junctions, triple points, etc. [26, 27].

A large number of reviews have been appeared over the years, containing these and many related ideas. We refer the interested reader to [20, 30, 35, 36, 38–40].

## 2 Industrial Printing

### *2.1 Physical Problem and Modeling Goals*

Industrial inkjet printing involves ejecting ink housed in a well through a narrow nozzle, which is then deposited on a material. The ink in the bath is expelled by an electro-actuator mechanism at the bottom, which quickly propels ink through the nozzle. The shape of the nozzle, the force and timing of the actuator, and the

properties of the ink are instrumental in determining the ultimate shape, delivery, and performance of the printing device.

This is a two-phase incompressible fluid flow problem, with the interface separating air and ink. Depending on the constituency of the ink, the flow can either be Newtonian or visco-elastic. Boundary conditions include both no-slip and no-flow at solid walls, and triple points where air-ink boundaries meets solid nozzle walls are subject to typical critical angle dynamics controlling slipping. While a common use for inkjet printers is in commercial home printing, over the past two decades a large number of sophisticated industrial applications have appeared, ranging from printing integrated circuits and the manufacture of display devices on through to construction of tissue scaffolding and layered manufacturing.

The goal of numerical simulation is to identify and optimize key aspects of the process, including

- Optimize the design of the nozzle and to control the actuator mechanism to aim, extend, and focus droplet delivery;
- Characterize wall wetting/non-wetting on the shape and separation of droplets;
- Determine and perhaps minimize the formation of secondary trailing droplets, which break off from the main ejected bubble as the fluid elongates, due to the effects of surface tension; and
- Understand how variations in viscosities and impurities affect droplet dynamics.

## 2.2 Equations of Motion and Computational Challenges

We solve for incompressible flow in a non-rectangular geometry, with no-slip and no-flow on walls, with air satisfying Newtonian flow and ink satisfying a visco-elastic Oldroyd-B model. The equations of motion [42–44], are given by

$$\begin{aligned} (Ink)\quad & \rho_1 \frac{D\boldsymbol{u}_1}{Dt} = -\nabla p_1 + \nabla \cdot (2\mu_1 \mathcal{D}_1) + \nabla \cdot \boldsymbol{\tau}_1 \,, \qquad \nabla \cdot \boldsymbol{u}_1 = 0 \,, \\ & \frac{D\boldsymbol{\tau}_1}{Dt} = \boldsymbol{\tau}_1 \cdot (\nabla \boldsymbol{u}_1) + (\nabla \boldsymbol{u}_1)^T \cdot \boldsymbol{\tau}_1 - \frac{1}{\lambda_1} \left( \boldsymbol{\tau}_1 - 2\mu_{p1} \mathcal{D}_1 \right) \,. \end{aligned} \tag{4}$$

$$(Air)\quad \rho_2 \frac{D\boldsymbol{u}_2}{Dt} = -\nabla p_2 + \nabla \cdot (2\mu_2 \mathcal{D}_2) \,, \qquad \nabla \cdot \boldsymbol{u}_2 = 0 \,. \tag{5}$$

$$\mathcal{D}_i = \frac{1}{2} \left[ \nabla \boldsymbol{u}_i + (\nabla \boldsymbol{u}_i)^T \right], \quad \boldsymbol{u}_i = u_i \boldsymbol{e}_r + v_i \boldsymbol{e}_z \,, \qquad i = 1, 2 \tag{6}$$

where, for the ink, $\boldsymbol{\tau}_1$ is the viscoelastic stress tensor, $\lambda_1$ is the viscoelastic relaxation time, $\mu_{p1}$ is the solute dynamic viscosity and subscript 2 refers to (Newtonian) air.

We use a level set method to track the air-ink interface, starting with the initial pressure disturbance in the reservoir: the fluid then moves through the nozzle and is then ejected into the ambient air, and then may separate into one or more droplets. We compute an approximate solution to the incompressible Navier-Stokes given above

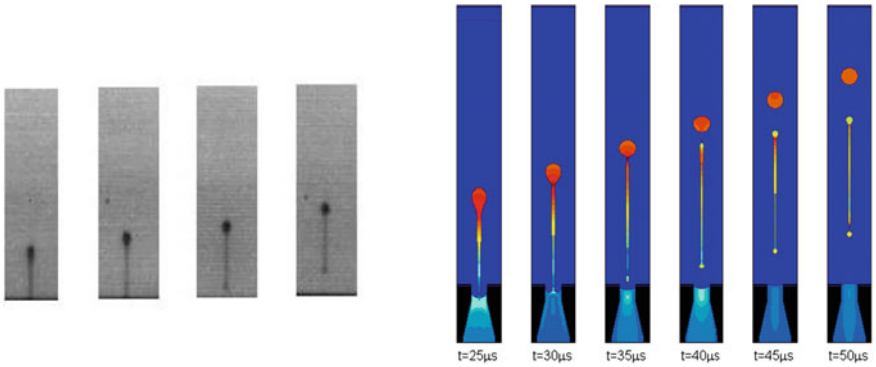


**Fig. 3** Left: Experimental profiles, showing ejected ink and satellite formation; note the formation of the trailing satellite droplet as the initial bubble stretches, and changes topology. Right: simulation of full ejection cycle (taken from [43]). Inflow pressure from an equivalent circuit model which describes the cartridge, supply channel, vibration plate, PZT actuator, and applied voltage. Fluid is an Epson dye-based ink, with critical advancing $\theta_a = 70°$ and receding $\theta_r = 30°$ contact angle, and with $\rho_1 = 1070$ kg/m$^3$, $\mu_1 = 3.34 \times 10^{-3}$ kg/m s, and $\sigma = 0.032$kg/s$^2$. The nozzle geometry has diameter 26 microns at opening and 65$\mu$m at bottom

in both phases simultaneously, with surface tension terms mollified to the right-hand-side as a forcing term. Thus, the solution accounts for both the ink velocity, the air-ink interface, and air currents induced in the air by the fluid ejection. We use a second order projection method [7–9] on a body-fitted logically rectangular mesh. Calculations are performed in both axi-symmetric two dimensions and full three-dimensional regimes. For details, see [42–44]. Figure 3 shows the results of both an experiment and simulation.

## 3 Droplet Formation and Electro-jetting

### *3.1 Physical Problem and Modeling Goals*

A large number of industrial problems involve microjetting and droplet dynamics, in which small droplets both move through small structures and also transport key materials, for example, in such areas as deposition of evaporation substances, delivery of biological materials, and substance separation.

Part of the challenge in computing these problems stems from the critical role of surface tension and shear forces, which often drive topological change, breakage, and merger in the evolving droplets. Level set methods, because of their ability to handle these structural changes, are particularly well-suited for computing droplet dynamics. Here, we summarize work on microjetting dynamics first presented in [10], see also [11–17].

Consider the dynamics of a thin tube of fluid as it pinches off due to surface tensions effects at a narrowing neck of the fluid (see Fig. 5), where mean curvature drives the interface inward until it breaks into two separate lobes of fluid. The pinch-off dynamics reveal considerable intricacy: as the droplet breaks, rapidly moving capillary waves on the surface cause instabilities and oscillations in the fluid lobes.

### *3.2 Equations of Motion*

Following the arguments in [11, 12], we model the fluid as incompressible and irrotational with a potential flow formulation. Euler's equation gives

$$\nabla \cdot \mathbf{u} = 0 \ \text{ in } \ \Omega(t) \tag{7}$$

$$\mathbf{u}_t + \mathbf{u} \cdot \nabla \mathbf{u} = \frac{-\nabla p}{\rho} + \textbf{bodyforces} \ \text{ on } \ \Gamma_t(\mathbf{s}). \tag{8}$$

Assuming irrotationality ($\nabla \times \mathbf{u} = 0$), the problem can then be written in terms of a fluid velocity potential $\mathbf{u} = \nabla\psi$, namely

$$\Delta\psi \ = 0 \text{ in } \Omega(t) \tag{9}$$

$$\psi_t + \frac{1}{2}(\nabla\psi \cdot \nabla\psi) + \frac{p - p_a}{\rho} = 0 \ \text{ on } \Gamma_t(\mathbf{s}), \tag{10}$$

where $p_a$ is the atmospheric pressure and $\rho$ is the fluid density.

As shown in [11, 12], this can be reformulated as

$$\mathbf{u} = \nabla\psi \ \text{ in } \ \Omega(t), \quad \Delta\psi = 0 \ \text{ in } \ \Omega(t) \tag{11}$$

$$\frac{D\psi}{Dt} = \frac{1}{2}\big(\nabla\psi \cdot \nabla\psi\big) - \frac{\gamma}{\rho}\big(\frac{1}{R_1} + \frac{1}{R_2}\big) \ \text{ on } \ \Gamma_t(\mathbf{s}) \ , \tag{12}$$

where $\Omega(t)$ is the fluid tube, $\Gamma_t(s)$ is the boundary of the tube, $R_1$ and $R_2$ are the principle radii of curvature, and $\gamma$ is the surface tension.

Although the potential $\psi$ is only defined on the interface, our plan is to build an extension of both the potential and the interface to all of space, so that we can then employ the level set methodology. This embedded implicit formulation then allows calculation of the fluid interface motion through pinch off, and can compute dynamics of the split fluid lobes.

These embeddings produce a new set of equations, namely

$$\mathbf{u} = \nabla\psi \ \text{ in } \ \Omega(t)$$
$$\Delta\psi(r,z) = 0 \ \text{ in } \ \Omega(t)$$
$$\phi_t + \mathbf{u}_{\text{ext}} \cdot \nabla\phi = 0 \ \text{ in } \ \Omega_D$$
$$G_t + \mathbf{u}_{\text{ext}} \cdot \nabla G = f_{\text{ext}} \ \text{ in } \ \Omega_D$$

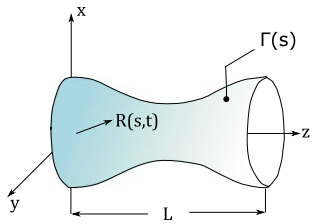


For details about the derivation of these equations, see [10–12].

### 3.3 Computational Challenges

The computational challenges that stem from these equations of motion lie in part on the delicate, sharp singularity at pinch off. The curvature becomes very large, and as soon as pinch off occurs, the two pieces of the neck retract very quickly. Constructing correct extension values for the velocity and the potential requires care as well.

We solve these equations through a time-cycle. Given values for the embedded implicit potential and level set function on a fixed background mesh, we construct the zero level set corresponding to the interface, place boundary element nodes on that interface, and then employ a boundary element method to find the new potential and associated velocity field, suitably extended. These nodes are then discarded, and the discrete grid values for the level set function, potential, and velocity are updated.

### 3.4 Example Results

Extensive numerical experiments are given in [12, 14]: the self-similar behavior of some variables near pinch-off time is checked within the computations and the computed scaling exponents agree with experimental and theoretical reported values. Here we review those results. Figure 4 shows a snapshot after pinch-off, revealing capillary surface waves on the undulating surface. Figure 5 shows the fine-scale structure of droplet dynamics after pinch-off.

### 3.5 Charged Droplet Separation

The above situation becomes considerably more complicated when the droplets are electrically charged, in which the droplet motion is driven by a background electrical field. Applications include electrospray ionization, electrospinning to produce fibers by drawing charged threads of polymers, particle deposition for nanostructures, drug delivery systems, and electrostatic rotary bell painting.

**Fig. 4** Droplet dynamics. Left, experiment taken from [41]. Right, level set calculation of surface capillary waves, taken from [12]

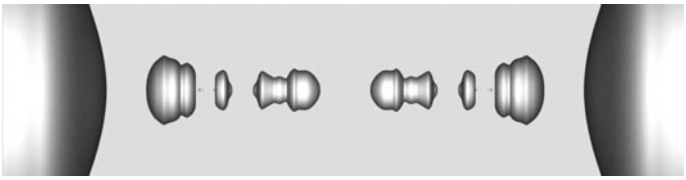

**Fig. 5** Simulation: fine-scale structure of droplet dynamics after pinch-off [12]

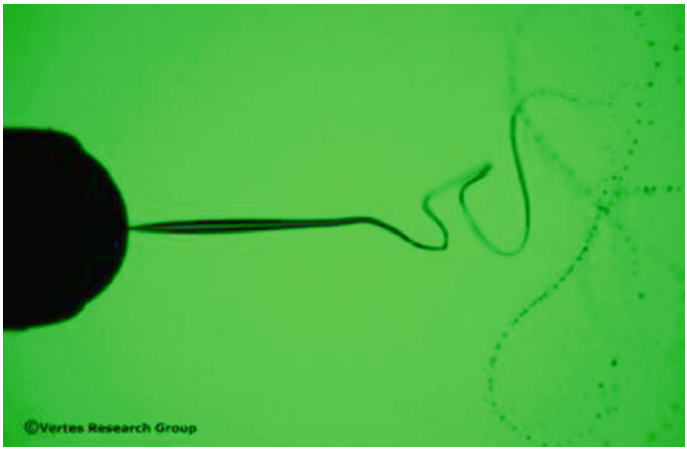


**Fig. 6** Experimental profile of electrically charged droplet motion [18]

The fundamental mechanism relies on the motion of an electrically conductive liquid in an electric field. The shape of the droplets starts to deform under the action of the electric field, afterwards the competition between inertial, surface tension and electric forces drives the dynamics, see Fig. 6.

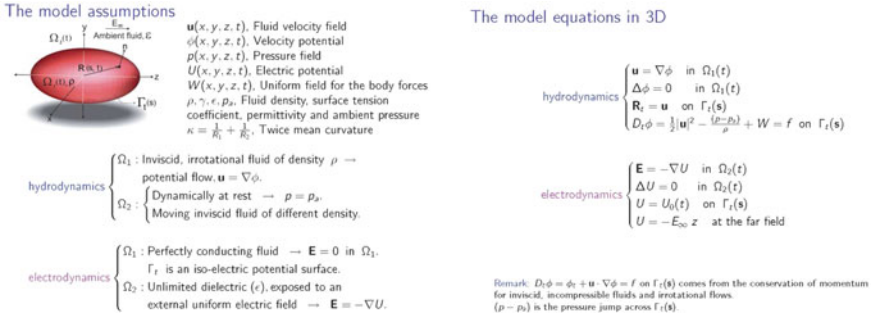


**Fig. 7** Equations for electrically charged droplet motion. Note: In the shown equations, the velocity potential is labelled $\Phi$ but is labelled by $\Psi$ in the main text

### *3.6 Equations of Motion and Computational Challenges*

The equations of motion are the previous potential formulation for droplet hydrodynamic motion, plus electrodynamics. We assume a perfectly conducting fluid and an unlimited dieletric exposed to an external uniform force field. Model equations from [16] are shown in Fig. 7.

Algorithmic challenges include accurate and reliable computation of the electric field and handling sharp breakup and fast ejection.

### *3.7 Example Results*

We show a numerical simulation [16] of a free charged droplet carrying a charge above the critical one, reproducing experimental results before and after jet emission. Figure 8 shows the focused droplet end from which charged tiny droplets are ejected.

## 4 Industrial Foams

### *4.1 Physical Problem and Modeling Goals*

Many problems involve the interaction of multiply-connected regions moving together. These include the mechanics and architecture of liquid foams, such as polyurethane and colloidal mixtures, and of solid foams, such as wood and bone.

The industrial applications of these problems are manifold. Liquid foams are key ingredients in industrial manufacturing, used in fire retardants and in froth flotation for separating substances. Solidification of liquid foams results in solid foams, which have remarkably strong compressible strength because of their pore-like internal structure; and include lightweight bicycle helmets and automotive absorbers.

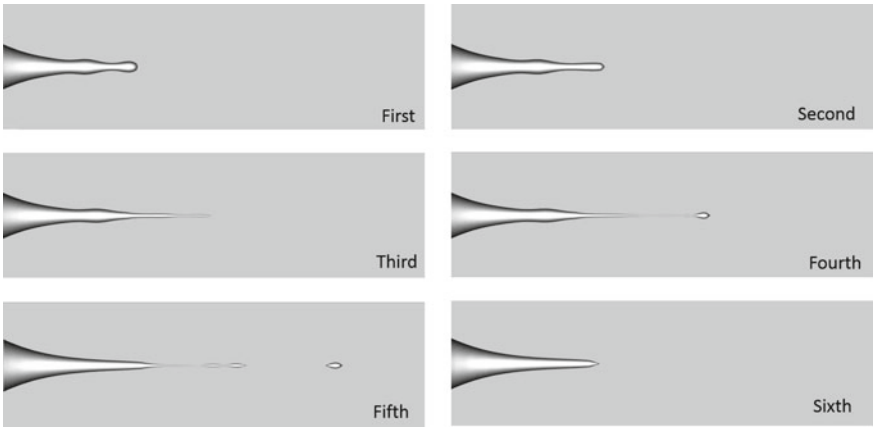


**Fig. 8** Time evolution of electrically charged droplet motion, from [16]

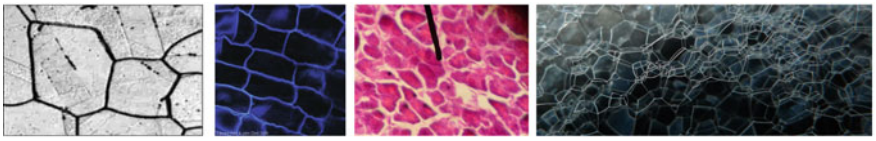


**Fig. 9** Examples of multiphase problems

In such problems, multiple domains share walls meeting at multiple junctions. Boundaries move under forces which depend on both local and global geometric properties, such as surface tension and volume constraints, as well long-range physical forces, including incompressible flow, membrane permeability, and elasticity.

Foam modeling is made challenging by the vast range of space and time scales involved [6]. Consider an open, half-empty bottle of beer. It may seem that nothing is happening in the collection of interconnected bubbles near the top, but currents in the lamellae separating the air pockets show slow but steady drainage. It can take tens to hundreds of seconds for the lamellae fluid to drain and then rupture, triggering an lamella explosion that retracts at hundreds of centimeters a second, after which the imbalanced configuration rights itself to a new stable structure in less than a second. Spatially, membranes are barely micrometers thick, while large gas pockets can span many millimeters or centimeters. All told, the biggest and smallest scales differ by roughly six orders of magnitude in space and time.

Another example comes from grain metal coarsening, in which surface energy, often associated with temperature changes, drives a system to larger structures. A third example comes from foam-foamed fiber networks, found in both industrial materials such as paper and biological materials, such as plant cells and tissues (Fig. 9).

In all of these engineering problems, understanding how such factors as pocket formation and distribution, tensile strengths, and foam architecture is a key part of producing mechanisms to optimize foam performance.

## *4.2 Computational Challenges*

Producing good mathematical models and numerical algorithms that capture the motion of these interfaces is challenging, especially at junctions where multiple interfaces meet, and when topological connections change. Methods have been proposed, including front tracking, volume of fluid, variational, and level set methods. It has remained a challenge to robustly and accurately handle the wide range of possible motions of an evolving, highly complex, multiply-connected interface separating a large number of phases under time-resolved physics.

The problem is exacerbated by the nature of the mathematical components that contribute to the dynamics, including: velocities dependent on such factors as curvature, normal directions and anisotropy; the solution of complex PDEs with jump conditions, source terms, and prescribed values at the interface and internal boundary conditions; area and volume-dependent integrals over phases; thermal effects and diffusion within phases; and balance of forces at complex junctions.

From a numerical perspective, some of the challenges stem from the vast time and space scales involved. Using the same spatial resolution to resolve the physics along interfaces is often impractical in the bulk phases. Sharp resolution of the interface and front-driven physical quantities located on the interface is required as input to the bulk PDEs. Accurately resolving interface junctures is critical in order to provide reliable values for the balances of forces at junctions.

All told, these lead to formidable numerical modeling challenges.

## *4.3 Voronoi Implicit Interface Methods*

Voronoi Implicit Interfaces Methods (VIIM), introduced in [26], provide an accurate, robust, and reliable way to track multiphase physics and problems with a large number of collected, interacting phases. They work in any number of space dimensions, represent the complete phase structure by a single function value plus indicator at each discretized element of the computational domain, couple easily to complex physics, and handle topological change, merger, breakage, and phase extinction in a natural manner. The underlying equations of motion that represent the evolving interface and complex physics may be approximated in either a finite difference or finite element framework. These equations couple level set methods for an evolving initial value Hamilton-Jacobi-type partial differential equation to a computational geometry-based Eikonal equation to produce a faithful phase representation. Here, we provide a brief review of the methods. For details, see [26].

The starting point is to consider a collection of non-overlapping phases which divide up the domain. The "interface" consists of places where these phases meet. In two dimensions, the simplest example is a single curve separating two phases. More complex structures might have multiple closed curves, each surrounding a separate phase, which meet in triple points or higher-order junctions. In three dimensions, the situation is far more complex.

The Voronoi Implicit Interface Method begins by characterizing the entire system through an implicit representation. For each point $x$ in the plane, define $\phi(x)$ as the distance to the closest interface. Additionally, define $\chi(x)$ as an integer-valued function which indicates the phase. By construction, the interface representing all possible boundaries is given as the zero level set $\{\phi(x) = 0\}$ of this unsigned distance function, and the indicator function reveals the type of phase.

Thus, for example, if $\phi(x) = 5$ and $\chi(x) = 4$, then we know that the point $x$ is located in phase 4, and the closest interface point is located a distance 5 away.

Starting with this unsigned distance function representation, we execute a two-step process. With interface speed $F$ in the normal direction:

- Advance $\phi$ through $k$ time steps using the standard level set methodology. That is, produce $\phi^{n+1}$ from $\phi^n$ by solving a discrete approximation to

$$\phi_t + F|\nabla\phi| = 0.$$

- Use the $\epsilon$ level sets of this time-advanced solution to reconstruct a new unsigned distance function. This is done by first computing the Voronoi interface from the $\epsilon$ level sets: this corresponds to the set of all points equidistant from at least two of the $\epsilon$ level sets from different phases, and closer to any of the non-equidistant phases. This Voronoi interface is then used to rebuild the unsigned distance function.

These two steps give the method its name: "Implicit Interface" because of the level set step for the time evolution, and "Voronoi" because of the reconstruction step used to rebuild the unsigned distance function and characteristic indicator function.

There are several things to note:

- The method works because of a comparison principle which, for a large fraction of physically reasonable flows built through the use of extension velocities (see [2]), keeps the zero level set trapped between the neighboring $\epsilon$ level sets. These $\epsilon$ level sets may be updated for a short period of time without suffering from the influence of the non-smooth ridge along the zero level set.
- The Voronoi reconstruction can be accomplished without explicit construction through two applications of fast Eikonal solvers [25, 37].
- Regions spontaneously disappear (appear) if they become small (large) enough so that an $\epsilon$-level set does not exist (can be constructed).
- Careful numerical algorithms can be devised to allow for any non-negative value for $\epsilon$, including $\epsilon = 0^+$.

For details, see [26, 27].

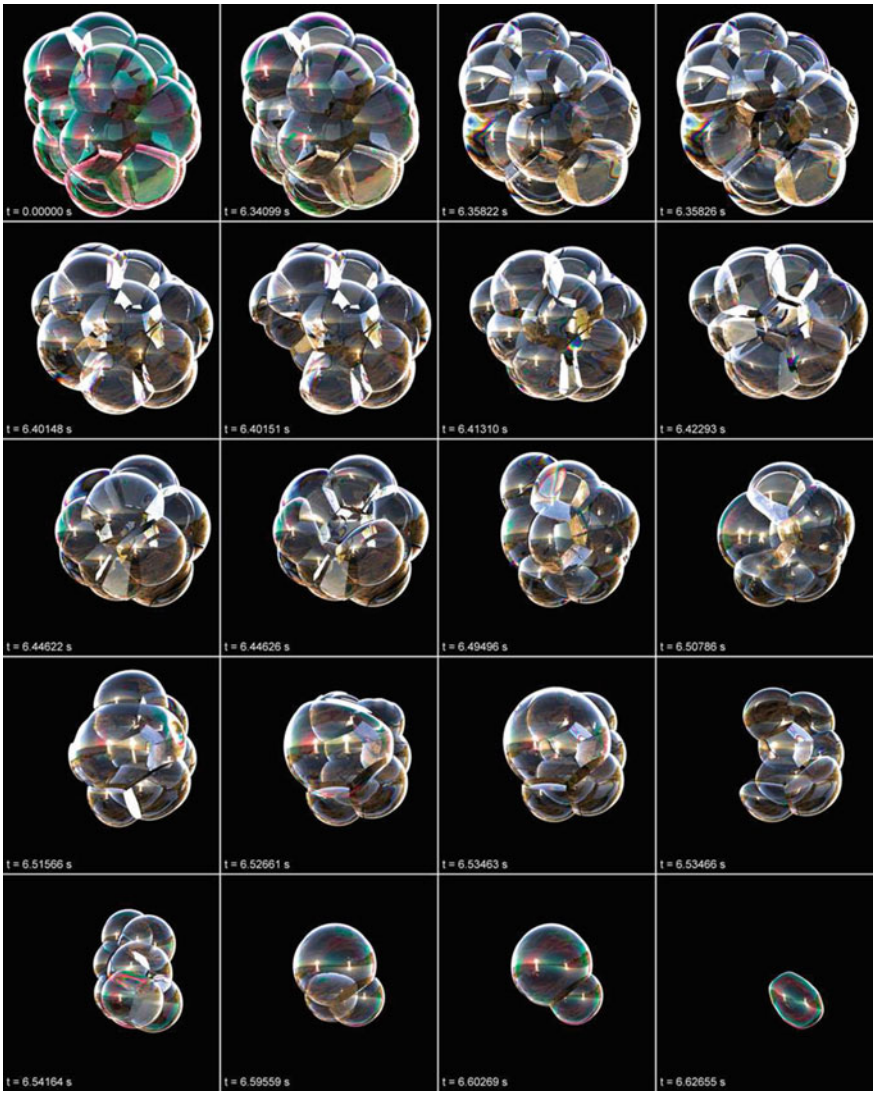


**Fig. 10** Collapse of a foam cluster, visualized with thin-film interference taken from [29]

## *4.4 Application of VIIM to Foam Dynamics*

Here, we review some current work applying VIIM to tracking the evolution of liquid foams. The vast time and space scales mean that one cannot compute over all scales simultaneously. Instead, we use a scale-separation model which allows us to divide the foam physics into three distinct stages.

We characterize the foam structures as represented by thin, interconnected membranes (lamellae) each surrounding pockets of air, and containing fluid. Membranes can share common walls, and fluid in each lamella drains toward common, shared Plateau borders that form a network of triple junctions and quadruple points. This drainage is slow, and once a membrane becomes too thin, it ruptures, causing the large air pockets to be out of macroscopic balance, which then readjust according to the equations of incompressible flow driven by interfacial forces along the lamellae.

These events can be thought of as taking places over different scales. The macroscopic air-fluid incompressible flow phase takes place over the whole domain, and evolves to an equilibrium relatively quickly. The lamellae drainage phase is slow, but takes place only over the very thin membrane walls. Rupture occurs very quickly.

In [28, 29], these three phases were used to develop a mathematical model and numerical simulation framework for foam evolution. During the macroscopic phase, a second order projection method is used to solve the incompressible Navier-Stokes equations on a rectangular mesh, with the interface smoothing its influence to the right-hand side through a mollified surface tension term. The individual lamellae are advanced under the incompressible flow by the Voronoi Implicit Interface Method, with the internal liquid transported by the method of characteristics. When the motion is almost gone, the model enters a different phase and assumes that the multi-phase configuration has essentially reached equilibrium; a fourth order PDE is then solved for thin film drainage, approximated through a discretized finite element triangulation. The final phase results from membrane rupture, idealized as an instantaneous disappearance of a lamella when a user-chosen minimal thickness is reached, which then redistributes the lamella liquid mass and sends the configuration into macroscopic disequilibrium.

### *4.5 Example Results*

An example of the complete dynamics developed in the multi-scale foam model is shown in Fig. 10, which shows the time evolution of a bubble cluster, starting from 26 separate bubbles and ending up in a single bubble. The bubble colors are computed from thin film interference determined by the computed fluid thickness in the lamellae.

## 5 Rotary Bell Painting in the Automotive Industry

In manufacturing settings, paints are frequently applied by an electrostatic rotary bell atomizer. Paint flows to a cup rotating at 10,000–70,000 rpm and is driven by centrifugal forces to form thin sheets and tendrils at the cup edge, where it then tears apart into dispersed droplets. Vortical structures generated by shaping air currents are key to shearing these sheets and transporting paint droplets. Advantages of this manufacturing process include the ability to paint at high volume and to achieve uniform consistency in the paint application.

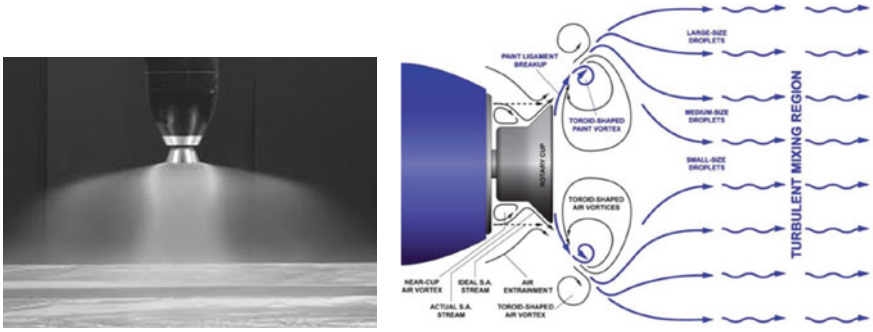


Schematic of paint flow and air currents [21] in rotary bell atomizing applications

Understanding the generation, size distribution, delivery, and adhesion of these paint droplets is a problem of considerable importance. For example, (a) much of the energy involved in automotive assembly is associated with the paint process; (b) a significant amount of paint does not attach to the cars and ends up as pollutants; and (c) 10–20% of automobiles need to be repainted due to aberrations in the process.

The goal of computational modeling of the rotary bell delivery system includes

- Optimizing the atomization process for higher paint flow rates to obtain more uniform and consistent atomization in the 30,000 to 60,000 rpm range.
- Studying the atomization process as a function of paint fluid properties (such as density, viscosity, and surface tension) and physical properties, such as inflow rates, bell rotation speeds and shaping air currents.
- Analyzing film dynamics, particularly in the immediate atomization zone adjacent to the cup edge, including the dynamics of filament formation and droplet size and distribution and their trajectories.

## *5.1 Computational Challenges*

The computational challenges posed by the painting delivery mechanism are formidable. The range of physical parameters is substantial. The droplet size ranges from 5 to 100 $\mu$m, the films are 10–50 $\mu$m thick, while the rotary bell diameter is on the order of centimeters. The cup rotates at 200 m/s, droplets breakup over microseconds, whereas droplet statistics requires milliseconds. As such, modeling requires tracking droplets across a wide range of length scales, paint fluid mechanics is subject to high centrifugal and Coriolis forces, and the impact of highly vortical air structures on film sheeting requires careful resolution.

From a computational point of view, these translate into daunting challenges:

- Interfaces are very contorted and complex.
- Very thin sheets of paint roll off, and then break into droplets.
- Fluid dynamics is highly three-dimensional with gas eddies playing a key role.
- Droplets are tiny, and break off and subsequently merge in highly complex ways.

- Mass conservation is important: tracking and accurately accounting for small droplets is critical, since all the paint ultimately breaks into such small objects.

These translate into several modeling/mathematical/algorithmic/numerical challenges which must be tackled in order to build a workable approach, including:

- *High-order accurate fluid solvers and sharp interface physics:* The standard level set approach to tracking two- or multi-phase fluid problems is to solve both the evolving level set equation and the Navier-Stokes equations on a background fixed mesh, smearing forces jump conditions, and discontinuities across the air/fluid interfaces through mollified delta functions into forcing terms on the background mesh. Because the droplets are so small, and because the viscosity/density jumps are so large, this approach is too inaccurate. Instead, we need to employ incompressible Navier-Stokes solvers that allow us to represent these forces sharply, by using implicitly defined meshes that adapt to the moving geometry of the liquid-gas interface.
- *Develop hybrid interface solvers coupled to high order fluid solvers.* Coupling these high-order fluid solvers to the interface dynamics requires building accurate methods to allow information transfer between the background Cartesian level set mesh and the unstructured interface-fitted mesh.
- *Non-Newtonian fluids:* Another complex challenge stems from the fact that paint is in fact non-Newtonian. One must carefully design and embed experimental shear stress models inside numerical calculations.
- *Mesh adaptivity:* In order to capture the shaping air currents and spinning bell, which occupy large length scales, as well as the smallest scales of droplets and thin films, we need to employ aggressive adaptive mesh refinement strategies.
- *Multi-core high performance computing:*This is an involved calculation, requiring small time steps, many mesh elements, and highly accurate elliptic solvers. Attention must be paid to parallel implementations on sophisticated computing architectures.

## 5.2 Level Set Methods and High-Order Multiphase Flow

The central problem in applying level set methods is that the equations of motion need to include jump conditions at the air-paint interface, e.g., droplet boundaries. The usual level set approach of "smearing" forces to a background mesh in order to provide source terms to the incompressible Navier-Stokes equations is problematic. The droplets can be so small, and the density/viscosity jumps so large and sharp, that this mollified approach does not provide the required accuracy.

Instead, we make use of an algorithmic technology building on implicitly-defined meshes [22–24]. There are several ideas at work in this approach:

- First, two-phase incompressible flow is solved using a discontinuous Galerkin (DG) approach, with a level set method used to track paint-air interfaces.

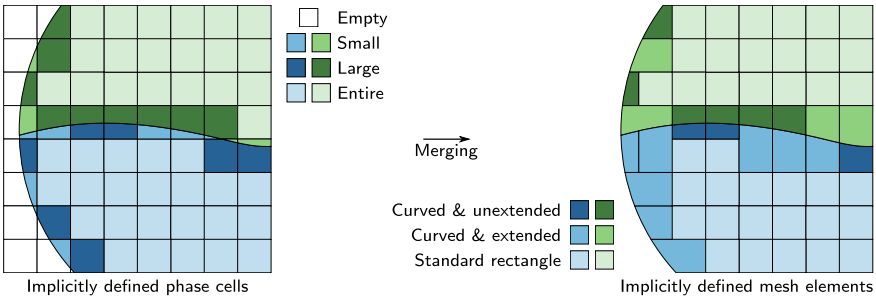


**Fig. 11** Implicitly defined meshes using multi-phase cell merging. Left: Phase cells, defined by the intersection of each phase (blue and green) with the cells of a background Cartesian/quadtree grid, are classified according to whether they fall entirely within one phase, entirely outside the domain, or according to whether they have a small or large volume fraction. Right: Small cells are merged with neighboring cells in the same phase to form a finite element mesh composed of standard rectangular elements and elements with curved, implicitly defined boundaries. Figures adapted from [23, 24]

- The level set method is solved using finite differences on a fixed background mesh in a time-evolving narrow-banded data structure.
- The zero level set corresponding to the paint-air boundaries, which cuts through the cells of a background octree grid, is used to drive a cell-merging procedure which creates an implicitly-defined mesh, whose element shapes exactly coincide with the curved geometry of the interface; see Fig. 11.
- This mesh is used to accurately incorporate the now body-aligned interface jump conditions in the DG solver.

**Adaptivity**: The next issue stems from the fact that there is a wide range of physical space scales involved in the process. The paint comes off the bell as a very thin film, and then breaks into small bubbles; as such, computing on a uniform mesh is impractical. Instead, we employ adaptively refined meshes wherein the mesh resolution adapts to such triggers as: (a) the distance to liquid-gas interface; (b) amount of curvature of interface; (c) the thickness of droplets, tendrils, films; and (d) the proximity to bell cup. See, for example, Fig. 12.

**High performance computing**: The above calculations are complex and the time step, spatial resolution, and physics make it impossible to model the entire bell. With a numerical framework targeting high performance computing facilities, using massively parallel MPI and OpenMP techniques, we can conduct high-resolution in-depth studies of rotary bell atomization on small wedges, about 5 degrees in angle, using tens of thousands of cores. In Fig. 13 we present one result from a large family of parameter studies. For further details, see [31].

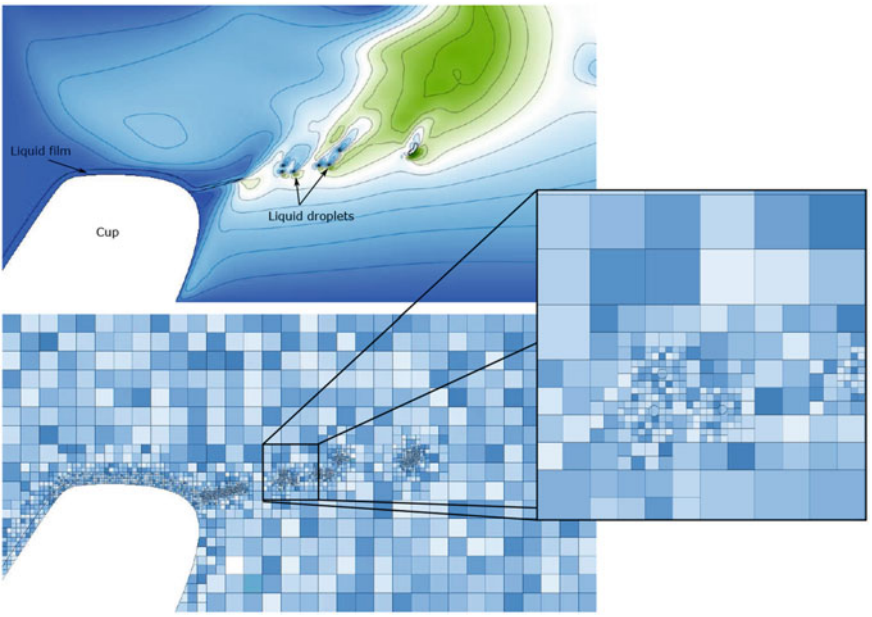


**Fig. 12** Adaptively refined meshing in the rotary bell atomizing problem


**Fig. 13** Three-dimensional model results of rotary bell atomization for time- and spatially-varying inflow film thickness, high mesh resolution, and shaping air currents simulating nozzle inlets. In each of the nine panels, two viewpoints at the same time frame are given: a top-down perspective and a side-on view to show the vertical drifting of the shedding droplets, being pushed upwards by the shaping air currents. The liquid surface is colored copper, with the bell cup situated beneath

## 6 Conclusions and Summary

We have tried to review a few examples in which the interface dynamics are a profound contributor to the efficiency of the industrial processes, and have focused on the application of level set methods for interface tracking to these problems. We have considered only a few contributions and works, and refer the interested reader to the referenced review articles.

**Acknowledgements** This work was supported in part by the Applied Mathematics Program of the U.S. DOE Office of Advanced Scientific Computing Research under contract number DE-AC02-05CH11231.

## References

1. Adalsteinsson, D., Sethian, J.A.: A Fast Level Set Method for Propagating Interfaces. J. Comp. Phys. **118**(2), 269–277 (1995)
2. Adalsteinsson, D., Sethian, J.A.: The fast construction of extension velocities in level set methods. J. Comp. Phys. 148:2–22
3. Adalsteinsson, D., Sethian, J.A.: A unified level set approach to etching, deposition and lithography I: algorithms and two-dimensional simulations. J. Comp. Phys. **120**(1), 128–144 (1995)
4. Adalsteinsson, D., Sethian, J.A.: A unified level set approach to etching, deposition and lithography II: three-dimensional simulations. J. Comp. Phys. **122**(2), 348–366 (1995)
5. Adalsteinsson, D., Sethian, J.A.: A unified level set approach to etching, deposition and lithography III: complex simulations and multiple effects. J. Comp. Phys. **138**(1), 193–223 (1997)
6. Adalsteinsson, D., Sethian, J.A.: Transport and diffusion of material quantities on propagating interfaces via level set methods. J. Comp. Phys **185**(1), 271–288 (2002)
7. Almgren, A., Bell, J.B., Szymczak, W.G.: A numerical method for the incompressible Navier-Stokes equations based on an approximate projection. SIAM J. Sci. Comput. **17**(2), 358–369 (1996)
8. Bell, J.B., Colella, P., Glaz, H.M.: A second-order projection method for the incompressible Navier-Stokes equations. J. Comp. Phys. **85**, 257–283 (1989)
9. Chorin, A.J.: Numerical solution of the Navier-Stokes equations. Math. Comp. **22**, 745 (1968)
10. Garzon, M., Bobillo-Ares, Sethian, J.A.: Some Free Boundary Problems in Potential Flow Regime using a Level Set Method. Recent Advances in Fluid Mechanics. Nova Publishers (2008)
11. Garzon, M, Gray, L.G., Sethian, J.A.: Wave breaking over sloping beaches using a coupled boundary integral-level set method. Interfaces Free Boundaries **7**(3), 229–239 (2008)
12. Garzon, M., Gray, L.G., Sethian, J.A.: Numerical simulation of non-viscous liquid pinch-off using a coupled level set-boundary integral method. J. Comput. Phys. **228**(17), 6079–6106 (2009)
13. Garzon, M., Gray, L.G., Sethian, J.A.: Axisymmetric boundary integral formulation for a two-fluid system. Int. J. Numer. Meth. Fluids **69**, 1124–1134 (2012)
14. Garzon, M., Gray, L.G., Sethian, J.A.: Simulation of the droplet-to-bubble transition in a two-fluid system. Phys. Rev. E **83**, 4 (2011)
15. Garzon, M., Gray, L.G., Sethian, J.A.: Droplet and bubble pinch-off computations using level sets. J. Comput. Appl. Math. **236**(12), 3034–3041 (2012)
16. Garzon, M., Gray, L.G., Sethian, J.A.: Numerical simulations of electrostatically driven jets from non-viscous droplets. Phys. Rev. E **89**, 033011 (2014)

17. Garzon, M., Johansson, A., Sethian, J.A.: A three-dimensional coupled Nitsche and level set method for electrohydrodynamic potential flows in moving domains. J. Comput. Phys. **309**, 1–386 (2016)
18. Nemes, P., Margineau, I., Vertes, A.: Spraying mode effect on droplet formation and ion chemistry on electrosprays. Anal. Chem. **79**, 3105–3116 (2007)
19. Osher, S., Sethian, J.A.: Fronts propagating with curvature-dependent dpeed: algorithms based on Hamilton-Jacobi formulations. J. Comp. Phys. **79**, 12–49 (1988)
20. Osher, S., Fedkiw, R.: Level Set Methods and Dynamic Implicit Surfaces. Springer, Berlin (2002)
21. Salazar, A.: Computational modeling of relevant automotive rotary spray painting process. In: Toda, K., Salazar, A., Saito, K. (eds.) Automotive Painting Technology: A Monozukuri-Hitozukuri Perspective (2012)
22. Saye, R.I.: High-order quadrature methods for implicitly defined surfaces and volumes in hyperrectangles. SIAM J. Sci. Comput. **37**(2), A993–A1019 (2015)
23. Saye, R.I.: Implicit mesh discontinuous galerkin methods and interfacial gauge methods for high-order accurate interface dynamics, with applications to surface tension dynamics, rigid body fluid-structure interaction, and free surface flow: Part I. J. Comput. Phys. **344**, 647–682 (2017)
24. Saye, R.I.: Implicit mesh discontinuous galerkin methods and interfacial gauge methods for high-order accurate interface dynamics, with applications to surface tension dynamics, rigid body fluid-structure interaction, and free surface flow: Part II. J. Comput. Phys. **344**, 683–723 (2017)
25. Saye, R.I.: High-order methods for computing distances to implicitly defined surfaces. Commun. Appl. Math. Comput. Sci. **9**, 107–141 (2014)
26. Saye, R.I., Sethian, J.A.: The Voronoi implicit interface method for computing multiphase physics. In: Proceedings of the National Academy of Sciences, 21 Nov 2011
27. Saye, R.I., Sethian, J.A.: Analysis and applications of the Voronoi implicit interface method. J. Comput. Phys. **231**(18), 6051–6085 (2012)
28. Saye, R.I., Sethian, J.A.: Multi-scale modelling of membrane rearrangement, drainage, and rupture in evolving foams. Sci. Mag. **340**(6133), 720–724 (2013)
29. Saye, R.I., Sethian, J.A.: Multiscale modelling of evolving foams. J. Comput. Phys. **315**, 273–301 (2016)
30. Saye, R.I., Sethian, J.A.: A review of level set methods to model interfaces moving under complex physics: recent challenges and advances. Handbook Numerical Anal. **21**(2020), 509–554 (2020)
31. Saye, R.I., Sethian, J.A.: Numerical simulation of rotary bell dynamics in automotive painting (Work in progress) (2020)
32. Sethian, J.A.: An analysis of flame propagation. Ph.D. dissertation, Department of Mathematics, University of California, Berkeley, CA (1982)
33. Sethian, J.A.: Curvature and the evolution of fronts. Comm. in Math. Phys. **101**, 487–499 (1985)
34. Sethian, J.A.: Numerical methods for propagating fronts. In: Concus, P., Finn, R. (eds.) Variational Methods for Free Surface Interfaces. Springer, New York (1987)
35. Sethian, J.A.: Level Set Methods and Fast Marching Methods. Cambridge University Press, Cambridge (1996)
36. Sethian, J.A.: Level Set Methods and Fast Marching Methods. Cambridge University Press, Cambridge (1999)
37. Sethian, J.A.: A fast marching level set method for monotonically advancing fronts. Proc. Nat. Acad. Sci. **93**(4), 1591–1595 (1996)
38. Sethian, J.A.: Evolution, implementation, and application of level set and fast marching methods for advancing fronts. J. Comp. Phys. **169**, 503–555 (2001)
39. Sethian, J.A., Adalsteinsson, D.: An overview of level set methods for etching, deposition, and lithography development. IEEE Trans. Semiconductor Dev. **10**(1), 167–184 (1997)

40. Sethian, J.A., Smereka, P.: Level set methods for fluid interfaces. Annual review of fluid mechanics **35**, 341–372 (2003)
41. Thorodssen, S.T.: Micro-dropslets and micro-bubbles. Imaging motion at small scales. Nus. Eng. Res. News **22**(1) (2007)
42. Yu, J.-D., Sakai, S., Sethian, J.A.: A coupled level set projection method applied to ink jet simulation. Interfaces Free Boundaries **193**(1), 275–305 (2003)
43. Yu, J.-D., Sakai, S., Sethian, J.A.: A coupled quadrilateral grid level set projection method applied to ink jet simulation. J. Compu. Phys. **206**(1), 227–251 (2005)
44. Yu, J.-D., Sakai, S., Sethian, J.A.: Two-phase viscoelastic jetting. J. Comp. Phys. **220**(2), 568–585 (2007)